Chemical Science

ROYAL SOCIETY OF CHEMISTRY

EDGE ARTICLE

View Article Online
View Journal | View Issue

Cite this: *Chem. Sci.*, 2025, **16**, 15037

All publication charges for this article have been paid for by the Royal Society of Chemistry

Facile and scalable synthesis of high-quality three-dimensional imine-linked covalent organic frameworks *via* crystalline intermediate transformation†

Jiaqiang Liu,[abc] Xin Su,[abc] Yan Xu,[d] Weiwei Tang,[*abc] Taimin Yang*[ef] and Junbo Gong[*abc]

Covalent organic frameworks (COFs), an emerging class of porous crystalline materials, have potential applications ranging from separation to catalysis. However, the harsh conditions required by the classical amorphous transformation route limit the scalability of COF synthesis, especially for three-dimensional covalent organic frameworks (3D COFs). Here, we propose a novel crystalline intermediate (CIM) transformation method that circumvents the stage of amorphous phase generation, enabling the facile and scalable synthesis of imine-linked 3D COFs. In contrast with the classical route of 3D COF synthesis, the CIM transformation process requires no deoxygenation or high-temperature treatment and offers gram-scalable production with efficient and controllable structure interpenetration. The transformation mechanism from a CIM to a 3D COF was investigated in detail, showing a direct crystal-to-crystal pathway. The structure of a CIM nanocrystal, determined by scanning three-dimensional electron diffraction (3DED), reveals a tightly packed diamond-like structure. Furthermore, this strategy was also successfully applied to the synthesis of other three imine-linked 3D COFs that leads to the discovery of two new COFs, demonstrating its broad applicability.

Received 27th June 2025
Accepted 11th July 2025

DOI: 10.1039/d5sc04741b

rsc.li/chemical-science

Introduction

Covalent organic frameworks (COFs) have been widely used in the fields of gas separation and storage,[1,2] catalysis,[3,4] environmental remediation,[5] drug release,[6,7] and optoelectronic devices[8,9] due to the two-dimensional (2D), three-dimensional (3D) regularly ordered array of basic building blocks and inherent porosity. Compared with 2D COFs, 3D COFs have larger specific surface area, interconnected channels, more stable physicochemical properties (less susceptible to damage by ultrasound, mechanical milling, *etc.*), and abundant available active sites.[10–14] However, most reports so far have focused on the synthesis and application of 2D COFs,[3,15,16] and 3D COFs are less explored due to their complex structures.[17,18]

Early boron-linked 3D COFs were synthesized under similar conditions to 2D COFs.[19,20] However, unlike boron linkages, imine-linked COFs are currently limited to the sealed-tube protocol (Scheme 1a) for the synthesis of 3D imine COFs due to poorer bond reversibility and greater sensitivity to oxygen at high temperatures.[21] While 2D imine COFs can be synthesized using mechanochemical iso-flux methods,[22,23] these methods are generally not applicable to 3D imine COFs. The system in the sealed-tube protocol is sensitive and requires an oxygen-free environment, usually achieved by several freeze–thaw cycles of degassing. Freeze–thaw cycling operations and torch sealing are inherently more hazardous operations. In addition, the need for an oxygen-free environment is extremely unsuitable for macro-preparation and places higher demands on the production equipment.[24–28] After balancing the reaction rate and crystallinity, the conversion of the initially amorphous polymer to crystalline 3D COFs still takes 2–9 days.[29–32] The harsh conditions and low space-time yield of this protocol make it difficult to achieve scale-up production of 3D COFs. Many efficient, green and scalable methods have been realised for the synthesis of 2D COFs,[4] but they are hardly applicable to the synthesis of

[a]*State Key Laboratory of Chemical Engineering, School of Chemical Engineering and Technology, Tianjin University, Weijin Road 92, Tian-jin, 300072, China*
[b]*Collaborative Innovation Center of Chemical Science and Engineering, Weijin Road 92, Tianjin, 300072, China*
[c]*Haihe Laboratory of Sustainable Chemical Transformations, Tianjin 300192, China*
[d]*Department of Chemistry, College of Sciences, Northeastern University, Shenyang, Liaoning 110819, China*
[e]*Department of Material and Environmental Chemistry Chemistry (MMK), Stockholm University, Svante Arrhenius väg 16C, Stockholm, SE-10691, Sweden*
[f]*Department of Physics and Astronomy, University of California, Irvine, California 92697, USA*

† Electronic supplementary information (ESI) available: Materials, methods, supporting figures, supporting tables, supporting references and crystallographic data for CIM-1 and CIM-2. CCDC 2389687 and 2389688. For ESI and crystallographic data in CIF or other electronic format see DOI: https://doi.org/10.1039/d5sc04741b

3D COFs, except for reversible, weakly stable boroxine-linked COFs.[33] For example, the *in situ* monitoring of the formation of mechanochemically imine-linked 2D COFs *via* template effects by Lotsch *et al.* has aroused our interest,[34] but unfortunately the process is not applicable to imine-linked 3D COFs. Due to the lack of a layered stacking structure, amorphous polymer intermediate transformation is considered to be the most plausible mechanism for the synthesis of dynamic covalently linked 3D COFs.[35] Unfortunately, this transformation is difficult to control, prone to multiphase issues, and sensitive to high temperatures, particularly in the case of covalent bonds like imine oxidation during the synthesis of imine-linked COFs.[35,36] Many efforts have been made to inhibit the formation of the initial amorphous substance,[37–39] but the 3D COFs obtained nowadays have a high degree of interpenetration and show obvious hydration, which is not conducive to the pursuit of high pore properties.[30,40,41] Therefore, a facile and scalable synthesis protocol with controllable interpenetration for 3D COFs is urgently desired.

Crystalline seed-mediated strategies are well-known in the synthesis of framework materials, such as metal–organic frameworks.[42,43] Previous studies attempted to regulate the synthesis process of 2D COFs using eutectic or hydrogen-bonded organic frameworks as intermediates.[44,45] Furthermore, the efficient synthesis of 2D imine COFs by mechanochemical methods has been achieved without the addition of auxiliary components.[22,23,34] However, the successful synthesis of 3D COFs using these methods has yet to be reported. Herein, we propose a novel crystalline intermediate (CIM) transformation protocol that enables the facile synthesis of a series of imine-linked 3D COFs (Scheme 1b). While this method involves a two-step synthesis, the synthetic process of the CIM route is more robust and controllable, improving the potential of industrial scale-up. The molecular and crystal structures of the crystalline intermediates were directly analysed by scanning 3DED, which is an emerging method for analysing beam-sensitive nanocrystals.[46–48] The structure of the intermediates can help us to optimise the synthesis of the final product. The crystal-to-crystal transformation pathway for the synthesis of 3D COFs from the CIM was unveiled, avoiding the formation of the initial amorphous polymer. Compared to the classical sealed-tube protocol, this novel CIM transformation protocol offers several clear advantages such as no need for deoxygenation operations, lower reaction temperature (90 °C), more efficient crystallisation (0.5 d), and easier scale-up (gram scale). Moreover, this novel protocol has been successfully extended to synthesize other three diamond (dia) net 3D COFs including two new COFs, demonstrating broad applicability. At last, the CIM strategy may provide ideas for developing new pathways for the multi-component construction and functionalisation of 3D COFs.

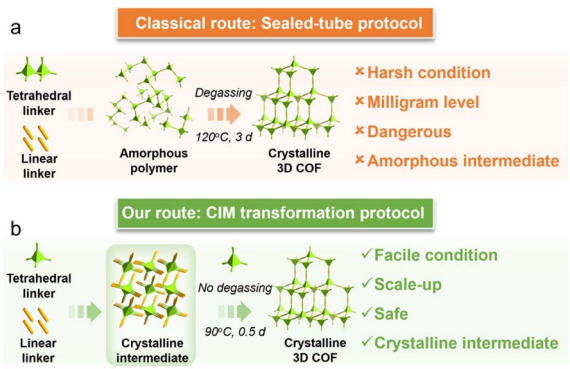

Scheme 1 Comparison of (a) the classical sealed-tube protocol with (b) the crystalline intermediate (CIM) transformation protocol for the synthesis of 3D COFs.

Results and discussion

Facile COF synthesis

COF-300, the first imine-linked 3D COF, was reported by Yaghi *et al.* in 2009.[29] The synthetic route involves the acid-catalysed imine condensation of the tetrahedral ligand tetrakis(4-aminophenyl)methane (TAM) and the linear ligand 1,4-phthaldehyde (TPA) within a sealed Pyrex tube using 1,4-dioxane as the solvent. After deoxidation, the reaction was carried out at 120 °C for 3 days to obtain the 5-fold interpenetrated dia-net COF-300-c5.[29] Obtaining the thermodynamically stable 7-fold interpenetrated isomer, COF-300-c7, requires another 6 day aging process prior to the synthetic procedure.[30] In contrast, our proposed CIM transformation protocol for the synthesis of 3D COFs operates under milder conditions, including lower temperatures, shorter heating times, and no need for deoxygenation. The crystalline product (COF-300) is obtained by adding equimolar amounts of the crystalline intermediate (CIM-1) and the tetrahedral ligand (TAM) in a relatively small amount of mixed solvent, followed by crystallisation at 90 °C for 12 hours. Furthermore, it is worth noting that the tetrahedral monomers are required for the transformation from CIM into COFs to make it more efficient and complete (Fig. S42†). The amount of CIM seeds will impact the kinetics of the transformation process, and the more CIM seeds added, the higher the crystallinity of the COF product will be (Fig. S43†). Besides, it was found that the synthesized COF product without the mechano-thermochemical treatment displays low crystalinity with poor porosity (Fig. S45 and S46†). The degree of interpenetration of COF-300 can be effectively controlled simply by whether or not stirring is performed during the CIM transformation process, with COF-300-c5 being obtained in the unstirred system and COF-300-c7 in the stirred system (Fig. 1a). Powder X-ray diffraction (PXRD) patterns show that the two interpenetrated heterostructures of COF-300 obtained by this approach have good crystallinity, which is consistent with literature reports (Fig. 1b and e).[29,30] Scanning electron microscopy (SEM) images showed that the two products had a uniform rod-like morphology, with the length of cof-300-c5 centred at around 300 nm (Fig. 1c), and the length of cof-300-c7 was 1–3 μm (Fig. 1f). N_2 adsorption–desorption isotherms at 77 K show that both interpenetrated frameworks exhibit evident adsorption hysteresis, consistent with the flexible nature of the framework (Fig. 1d and g). Similar observations were also reported previously, attributed to the deformation in

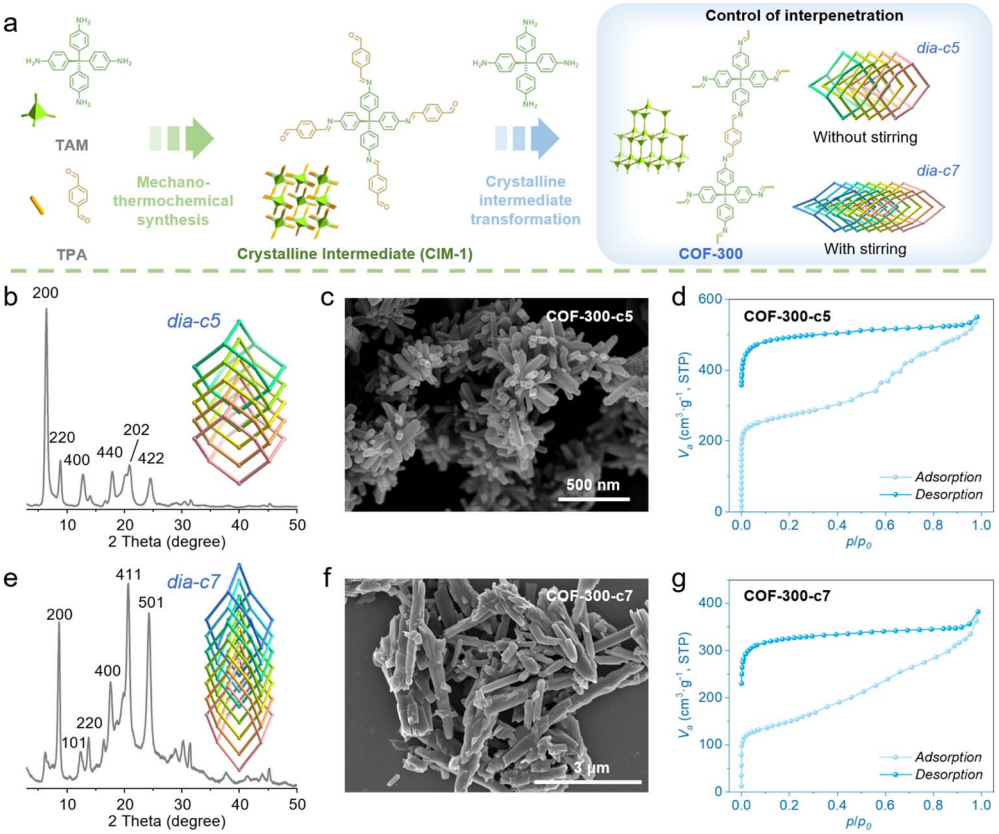

Fig. 1 Facile synthesis of 3D COFs and their structural, morphological and pore characterisation. (a) Synthesis route of two interpenetrated isomers of COF-300 *via* the CIM transformation approach. (b) PXRD pattern of COF-300-c5. (c) SEM image of COF-300-c5. (d) N_2 adsorption–desorption isotherms of COF-300-c5. (e) PXRD pattern of COF-300-c7. (f) SEM image of COF-300-c7. (g) N_2 adsorption–desorption isotherms of COF-300-c7.

node geometry, displacements between frameworks and conformational changes in the organic linkers.[37,49] The pore volume of COF-300-c5 was measured to be $V_p = 0.85$ cm^3 g^{-1} for $P/P_0 = 0.98$, which is comparable to that synthesised by the classical protocol,[29,50] and the pore volume of COF-300-c7 was $V_p = 0.59$ cm^3 g^{-1} for $P/P_0 = 0.98$. The Brunauer–Emmett–Teller (BET) surface areas of dia-c5 and dia-c7 COF-300 were determined to be 938 m^2 g^{-1} and 520 m^2 g^{-1}, respectively. These values are clearly superior to those obtained by other preparation methods such as the ventilation-vial synthesis method and amino acid assisted method detailed in Table S4.† The large surface area of COF-300 synthesized by our proposed CIM method is presumably due to the high crystallinity contributed by the slow release of crystalline intermediates. The typical dynamic pore characteristics of COF-300 from the CIM, *i.e.*, changing the pore size as the guest is absorbed or removed, are promising for applications in gas storage and separation.[51]

Crystalline intermediate (CIM)

The crystalline intermediate was pre-synthesised by a solvent-free mechano-thermochemical method, *i.e.*, combining mechanical milling with thermal treatment, following our previous work on solvent-free coordinated MOFs.[52] The process contains a mechanochemical stage to achieve rapid conversion of feedstock to covalent polymers and a heat treatment stage to achieve crystallisation of amorphous polymers to crystalline intermediates. This process clearly differs from the observation of crystalline intermediates in the mechanochemical synthesis of 2D COFs.[34] Notably, we did not observe the formation of crystalline 3D COFs/crystalline intermediates after sufficient mechanical milling, but amorphous polymers were observed, indicating the use of mechanochemical limitations alone. In this way, the crystalline intermediate CIM-1 for the synthesis of COF-300 was efficiently prepared by using an excess of linear units *via* a Schiff base condensation reaction. Specifically, the tetrahedral ligand TAM and an excess of linear monomer TPA were mixed and ground for 30 min and then transferred to a reactor for crystallisation at 120 °C for 24 h. The yellowish powder of highly crystalline CIM-1 was obtained after washing and drying. The synthetic crystallization route of CIM-1 involves the initial formation of amorphous polymers and then transformation into crystalline products, as disclosed from the changes in crystallinity, functional groups and morphology at each stage (Fig. S13–S18†). In the mechanical milling stage, the amorphous phase with no regular morphology was obtained (Fig. S18†). The FT-IR spectrum (Fig. S17†) shows the characteristic imine bonding peaks at around 1620 cm^{-1}, indicating the formation of amorphous polymers linked by imine bonds.

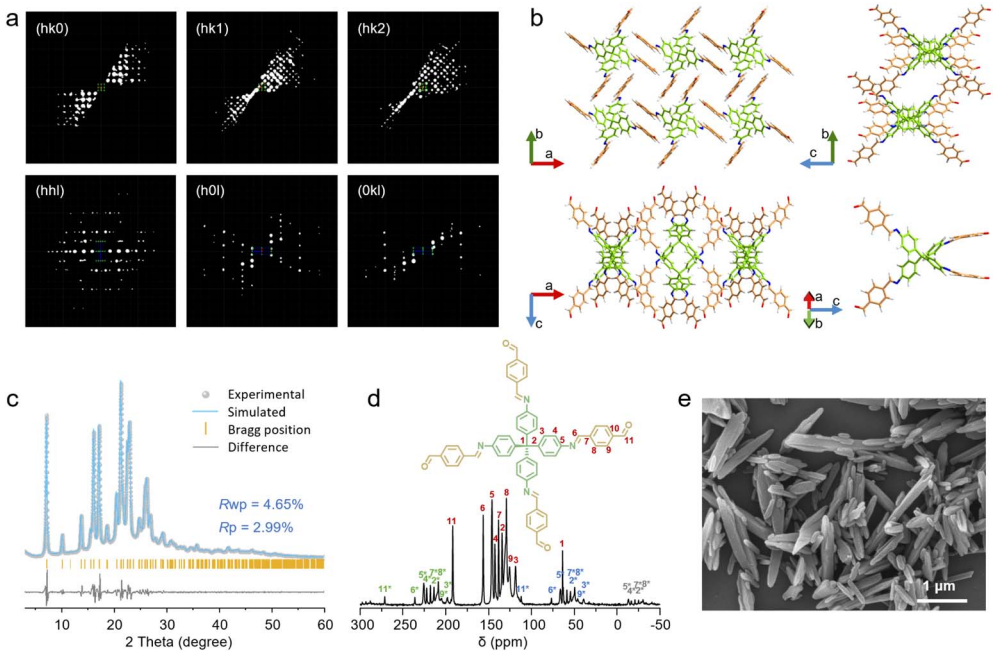

Fig. 2 Structural and morphological characterisation of CIM-1. (a) The 3D reciprocal lattice of CIM-1 reconstructed from the RED data. (*hk*0), (*hk*1), (*hk*2), (*hhl*), (*h*0*l*) and (0*kl*) slices cut from the reconstructed reciprocal lattice. (b) The crystal structure model of CIM-1 based on the RED data at 89 K. (c) Indexed PXRD pattern of CIM-1 and the Pawley fitting from the modeled structure. (d) Solid-state ^{13}C CP-MAS NMR spectrum (the asterisks denote the spinning sidebands) and (e) SEM image of CIM-1.

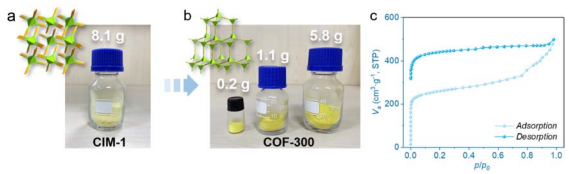

Fig. 3 Gram-scale synthesis of CIM-1 and COF-300. (a) Laboratory gram-scale synthesis of CIM-1. (b) Laboratory step-by-step gram-scale synthesis of COF-300. (c) N_2 sorption isotherms of gram-scale-synthesized COF-300 at 77 K.

The later heat treatment process results in the gradual transformation of the amorphous phase into the crystalline CIM-1 (Fig. S14 and S18†).

CIM-1 displays rod-like morphology with a length-size distribution of 0.5–3 μm (Fig. 2e). High resolution transmission electron microscopy (HR-TEM) images showed clear lattice fringes, confirming the long-range ordered structure of CIM-1 (Fig. S11†). Scanning 3DED was performed under low temperature conditions (89 K), and the 3D reciprocal lattice was reconstructed and visualised (Fig. 2a).[53] From the 3D reciprocal lattice, the unit cell was identified as a body-centred tetragonal cell with $a = b = 24.80$ Å, and $c = 7.86$ Å. The CIM-1 crystal diffracted to a very high resolution (0.8 Å), and its structure was solved *ab initio* from the 3D ED data in space group $I4_1/a$ (Table S1†). In CIM-1 crystals, each Schiff base molecule consists of a tetrahedral ligand (TAM) linked to four linear ligands (TPA) *via* imine bonds, which are stacked in the interpenetrated form of dia-like COFs, forming a non-porous network structure through non-covalent interactions (Fig. 2b). The N_2 adsorption–desorption isotherm of CIM-1 demonstrates close packing properties (Fig. S9†). The structure of CIM-1 was further subjected to full profile pattern matching (Pawley) refinement with PXRD data measured at room temperature, yielding $a = b = 24.705$ Å and $c = 7.984$ Å refined cell parameters with $R_{wp} = 4.65\%$ and $R_p = 2.99\%$ (Fig. 2c). Intramolecular imine linkages and unlinked aldehyde groups from linear monomers in the Schiff base CIM-1 were confirmed by using the solid-state ^{13}C CP-MAS NMR spectrum and FT-IR spectroscopy (Fig. 2d and S10†). The extra peaks (asterisks) which appeared in the solid-state ^{13}C CP-MAS NMR spectrum were due to the spinning sidebands, manifested as very similar patterns (Fig. 2d).[30] *In situ* PXRD studies show no attenuation of the diffraction peaks from CIM-1 in air below 300 °C (Fig. S12†). Thermogravimetric analysis experiments under a nitrogen atmosphere show that the weight loss started at 320 °C and the first maximum weight loss rate was at 350 °C (Fig. S13†). This gives CIM-1, with its good thermal stability, an advantage over virgin materials that are susceptible to oxidation.

Transformation process from the CIM to COFs

To investigate the details of the transformation of CIM-1 into COF-300, the products were taken at different times and analysed for the structure, morphology and yield. Without stirring, CIM-1 was completely converted to highly crystalline COF-300-c5 within 12 h (Fig. S19–S22†). In particular, when the transformation was carried out for 1 h, the PXRD patterns and SEM images showed a weakening of the characteristic peaks of CIM-1 accompanied by the appearance of a small amount of the crystalline phase COF-300-c5 (Fig. S19 and S20†). The presence of the

two phases, *i.e.*, CIM-1 and COF-300-c5, was clearly shown in the reaction system at 3 h and 6 h, and no amorphous intermediate phase appeared. The conversion from CIM-1 to COF-300-c5 was completed after 12 h (Fig. S19 and S20†). Throughout the transformation process, the characteristic –CHO absorption peak representing the intermediate CIM-1 in the FT-IR spectrum weakened and the characteristic –CH═N– peak gradually strengthened (Fig. S21†).[54] Satisfactorily, the yield gradually increased to 93% (Fig. S22†). The transformation of CIM into crystalline COFs is attributed to the low solubility of the intermediates, which effectively controls the reaction rate of polymerisation and avoids the rapid formation of an amorphous phase in the new system with a high concentration of reactants (Table S2†). Correspondingly, with stirring, CIM-1 first synthesised the dynamically dominant COF-300-c5, which later transforms into COF-300-c7 (Fig. S23–S26†). The stirring process promotes the formation of the thermodynamically stable phase COF-300-c7. In classical synthetic methods, the ageing process (typically a few days) was employed to achieve phase transformation from the metastable c5 form to the thermodynamically stable c7 form.[30] In this study, a similar but more rapid transformation process from c5 to the c7 form was observed under stirring conditions, which is presumably associated with the acceleration of mass and momentum transfers, favoring the transition of low-interpenetrating crystalline forms across the phase transition energy barrier to thermodynamically stable high-interpenetrating crystalline forms. Here, the success in effectively controlling the degree of interpenetration of COFs by balancing the dynamically and thermodynamically dominant synthesis pathways has important implications for the tailoring of specific functional porous frameworks.

Scalable CIM and COF synthesis

Based on the facile synthetic conditions of the method, the transformation route from CIM to COFs has potential for large-scale production. First, CIMs with high crystallinity can be easily prepared gram for gram by the mechano-thermochemical method in the absence of reaction solvents (Fig. 3a and S27†), producing a theoretical yield of up to 96% for CIM-1. The synthesis of COF-300-c5 from CIM-1 easily achieved stepwise scale-up (Fig. 3b and S28†). The average yield was maintained above 92%, much higher than that of the classical amorphous route, typically 63%.[29,30] The average space-time yield was 322 kg m^{-3} day^{-1}, which was more than 100 times higher than that of the classical route.[29,30] N_2 adsorption–desorption isotherms showed that the pore volume of the gram-scale synthesised COF-300 remained above 92% (Fig. 3c). It is noteworthy that in the design of porous materials, low interpenetrated frameworks

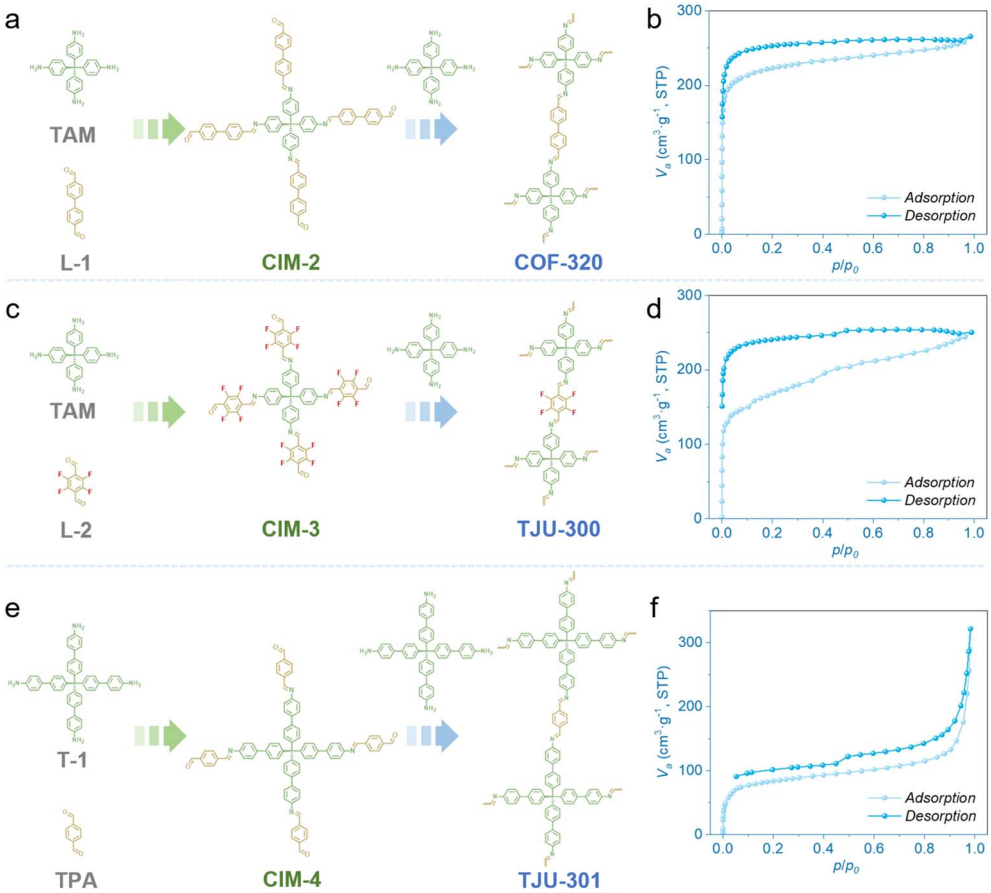

Fig. 4 The CIM transformation route to synthesise multiple dia net imine-linked 3D COFs. Synthesis routes *via* CIMs for (a) COF-320, (c) TJU-300, and (e) TJU-301. N_2 adsorption–desorption isotherms at 77 K of (b) COF-320, (d) TJU-300, and (f) TJU-301. (L-1 = 4,4′-biphenyldicarboxaldehyde; L-2 = 2,3,5,6-tetrafluoroterephthalaldehyde; T-1 = 4′,4‴,4⁗,4⁗′⁗′-methanetetrayltetrakis(([1,1′-biphenyl]-4-amine))).

with larger pore space are preferred. Here, we successfully positioned the kinetically advantageous low interpenetration phase through our CIM transformation strategy and achieved the first scale-up preparation of COF-300-c5 (Table S4†).

Universality of the CIM transformation protocol

The broad applicability of the proposed CIM transformation strategy was successfully demonstrated for the synthesis of other three imine-linked 3D COFs. First, another crystalline intermediate CIM-2 was synthesised by the mechano-thermochemical method using 4,4′-biphenyldicarboxaldehyde (L-1) and TAM, and the crystal structure was fully determined. Using the CIM transformation pathway, COF-320 was then further synthesised from CIM-2. Next, TJU-300 (TJU is an abbreviation for Tianjin University) and TJU-301 were synthesised in the same way (Fig. 4a, c and e).

To further clarify the structure of the crystalline intermediates, CIM-2 microcrystals were directly analysed by scanning 3DED (Fig. S29 and Table S5†), and the molecular structure and stacking pattern is similar to that of CIM-1 (Fig. S30†). The experimental PXRD pattern is in rigorous agreement with the calculated results (Fig. S31†). It is worth noting that during the conversion from CIM-2 to COF-320, the PXRD patterns show that the characteristic peaks of COF-320 have appeared before the disappearance of the CIM-2 diffraction peaks, and the characteristic broad peaks of amorphous polymers are not obvious (Fig. S34†). This again suggests that the transformation from CIM-2 into COF-320 follows the crystal-to-crystal pathway with high crystallinity. The crystal structures of TJU-300 and TJU-301 were simulated according to PXRD patterns. Geometric energy minimisation calculations were performed, using 5-fold and 11-fold interpenetrated nets, respectively, and verified with the generic formula for dia networks (Fig. S36, S37, S39, S40 and Tables S6, S7†).[30] N_2 adsorption–desorption isotherms showed that COF-320 and TJU-300 presented similar flexible pore characteristics to COF-300, with pore volumes of $V_p = 0.41$ cm^3 g^{-1} for $P/P_0 = 0.98$ and $V_p = 0.38$ cm^3 g^{-1} for $P/P_0 = 0.99$ (Fig. 4b and d). TJU-301 exhibits a sharp increase in gas adsorption at low pressure $0.1P/P_0$, corresponding to its 2.0 nm pore size, and $0.8–1.0P/P_0$ exhibits mesoporous properties, which is the result of crystal agglomeration, with a pore volume of $V_p = 0.49$ cm^3 g^{-1} for $P/P_0 = 0.98$ (Fig. 4f and S41†). Moreover, the BET surface areas of COF-320, TJU-300 and TJU-301 were determined to be 768 m^2 g^{-1}, 575 m^2 g^{-1} and 291 m^2 g^{-1}, respectively. This demonstrates the generalizability of the proposed method in synthesizing porous framework materials. Compared to other scale-up methods,[37–39] 3D COFs synthesised by the CIM transformation pathway, such as COF-300-c5 and TJU-300, prefer to generate networks without hydration, which offers advantages in reducing activation time and designing high porosity COFs.

Conclusions

In summary, we report a novel crystalline intermediate (CIM) transformation method for the facile and scalable production of imine-linked 3D COFs. While crystalline intermediates have previously been observed in the mechanochemical synthesis of 2D COFs, the direct synthesis of high-quality 3D imine-linked COFs has been demonstrated to be impossible by this method. Instead, we utilize the mechano-thermochemical method to obtain crystalline intermediates, and then make full use of the facile crystal-to-crystal transformation pathway, thus avoiding using deoxygenation and high temperature while producing 3D COFs with much more efficiency and productivity, in contrast to the classical sealed-tube protocol of 3D COFs. We successfully achieved the gram-scale production of highly crystalline COF-300 with controllable structure interpenetration. The choice between producing COF-300-c5 or COF-300-c7 structures can be easily controlled by simply stirring or not during the transformation process from CIM into COFs. Furthermore, the broad applicability of the proposed novel method was demonstrated for the synthesis of other three imine-linked 3D COFs, *i.e.*, COF-320, TJU-300 and TJU-301. Overall, our CIM transformation approach unlocks new possibilities for the large-scale, efficient production of COFs under mild conditions that were previously unattainable. Using the CIM as an intermediary paves the way for future design and development of multi-component 3D COFs with high crystallinity, accelerating the discovery and large-scale production of 3D COF materials.

Experimental section

Materials

All starting materials were commercially purchased and used without further purification. 1,4-phthalaldehyde (TPA, >98%), 4,4′-biphenyldicarboxaldehyde (L-1, >97%), 2,3,5,6-tetrafluoroterephthalaldehyde (L-2, >98%), tetrakis(4-aminophenyl)methane (TAM, >95%), and 4′,4‴,4⁗,4⁗′-methanetetrayltetrakis([1,1′-biphenyl]-4-amine)) (T-1, >98%) were purchased from Bide Pharmatech Ltd. Tetrahydrofuran and 1,4-dioxane were purchased from Sigma Aldrich.

Synthesis of CIM-1

First, 38 mg of TAM (0.1 mmol) and 134 mg of TPA (1 mmol) were mixed and ground in a mortar for 30 minutes. This mixture was then transferred to a 25 mL PTFE reactor and heated at 120 °C for 24 hours. After cooling to room temperature, the product was collected, washed with tetrahydrofuran, and dried under vacuum at 120 °C overnight to give a light-yellow powder, CIM-1.

Synthesis of COF-300 from CIM-1

First, 38 mg of TAM (0.1 mmol) and 84.4 mg of CIM-1 (0.1 mmol) were dispersed in 1 ml of the solvent mixture ($V_{1,4\text{-Dioxane}} : V_{water} : V_{acetic\ acid} = 7.5 : 5 : 1$) in a 10 ml pressure resistant glass vial. The reaction system was directly heated at 90 °C for 12 hours without stirring. After cooling to room temperature, the solid product was collected, washed with tetrahydrofuran, and dried under vacuum at 120 °C overnight to produce the yellow powder COF-300-c5. Following the same procedure, the heating process with stirring produced COF-300-c7.

Characterization of the CIM and COFs

Powder X-ray diffraction (PXRD) data of all samples in this work were collected on a Rigaku D/MAX 2500 X-ray diffractometer using Cu-Kα radiation ($\lambda = 1.54178$ Å). The voltage and current were 40 kV and 200 mA, respectively. Powder samples used for refinement of structures were scanned in the 2θ range of 3–60° at a scan rate of 5° min^{-1}. *In situ* PXRD test results were collected by varying the temperature in air from 50 °C to 375 °C with a 5 °C min^{-1} ramp-up. The FT-IR spectra of the samples were collected on a Bruker alpha ATR-FTIR instrument (Germany) over the wavenumber range from 400 to 4000 cm^{-1} at a resolution of 4 cm^{-1} using 64 scans. The ^{13}C MAS NMR spectra of the samples were collected on a 500 MHz Bruker spectrometer equipped with the standard cavity CP MAS and probe-BL4. The morphologies of the samples were characterized using a scanning electron microscope (SEM, Hitachi SU-8010). The characterization studies of lattice diffraction and the internal mesoporous structure of the samples were carried out on a JEM-F200 field emission transmission electron microscope (TEM). Thermogravimetric (TG) analysis was carried out on a model TGA 1/SF thermogravimetric analysis system (Mettler Toledo, Switzerland).

Nitrogen adsorption–desorption isotherm measurements

The N_2 adsorption–desorption isotherms of the samples were evaluated on an Autosorb IQ2 surface area and pore size analyser at 77 K after vacuum degassing at 120 °C for 12 hours. The pore size distribution of the materials was analyzed using the Non-Local Density Functional Theory (NLDFT) method.

Scanning three dimensional electron diffraction

Scanning three dimensional electron diffraction (3DED) was conducted in a Thermal Fisher Themis-Z TEM operated at 300 kV. The microscope was switched to STEM mode and the electron beam is defocused to a nearly parallel state. A video stream from the HAADF detector was displayed during data collection for crystal tracking, and electron diffraction patterns were acquired on a Gatan OneView IS detector (4096 × 4096, 15 μm in pixel size) when the stage was rotated continuously from −50° to +50°. The scanning 3DED datasets were processed by XDS, and the structures were solved *ab initio* from the output HKL files using SHELXT and refined by SHELXL.

Data availability

The data supporting this article have been included as part of the ESI. Crystallographic data for CIM-1 and CIM-2 have been deposited at the CCDC under 2389687 and 2389688.†

Author contributions

J. Liu: conceptualization, data curation, formal analysis, methodology, writing-original draft. X. Su: data curation. Y. Xu: writing-review & editing. W. Tang: funding acquisition, investigation, writing-review & editing. T. Yang: funding acquisition, investigation, writing-review & editing. J. Gong: project administration, supervision.

Conflicts of interest

There are no conflicts to declare.

Acknowledgements

This work was supported by the National Natural Science Foundation of China (NNSFC 22278300 and 22478284), the Innovative Research Group Project of the National Natural Science Foundation of China (21621004), the Natural Science Foundation of Tianjin (22JCZDJC00040), the Marie Skłodowska-Curie grant agreement (101146059), the Royal Swedish Academy (CH2022-0015 and PH2022-0021) and Swedish Research Council Formas (2022-02778).

References

1 A. Giri and P. E. Hopkins, *Nano Lett.*, 2021, **21**, 6188–6193.
2 S. T. Emmerling, J. Maschita and B. V. Lotsch, *J. Am. Chem. Soc.*, 2023, **145**, 7800–7809.
3 Z. Alsudairy, N. Brown, A. Campbell, A. Ambus, B. Brown, K. Smith-Petty and X. Li, *Mater. Chem. Front.*, 2023, **7**, 3298–3331.
4 A. Dey, S. Chakraborty, A. Singh, F. A. Rahimi, S. Biswas, T. Mandal and T. K. Maji, *Angew. Chem., Int. Ed.*, 2024, **63**, e202403093.
5 N. Zhang, A. Ishag, Y. Li, H. Wang, H. Guo, P. Mei, Q. Meng and Y. Sun, *J. Clean. Prod.*, 2020, **277**, 123360.
6 L. Ge, C. Qiao, Y. Tang, X. Zhang and X. Jiang, *Nano Lett.*, 2021, **21**, 3218–3224.
7 V. Sridhar, E. Yildiz, A. Rodríguez-Camargo, X. Lyu, L. Yao, P. Wrede, A. Aghakhani, B. M. Akolpoglu, F. Podjaski, B. V. Lotsch and M. Sitti, *Adv. Mater.*, 2023, **35**, 2301126.
8 X. Ren, G. Liao, Z. Li, H. Qiao, Y. Zhang, X. Yu, B. Wang, H. Tan, L. Shi, X. Qi and H. Zhang, *Coord. Chem. Rev.*, 2021, **435**, 213781.
9 S. Bag, H. S. Sasmal, S. P. Chaudhary, K. Dey, D. Blätte, R. Guntermann, Y. Zhang, M. Položij, A. Kuc, A. Shelke, R. K. Vijayaraghavan, T. G. Ajithkumar, S. Bhattacharyya, T. Heine, T. Bein and R. Banerjee, *J. Am. Chem. Soc.*, 2023, **145**, 1649–1659.
10 Y. Xiao, Y. Ling, K. Wang, S. Ren, Y. Ma and L. Li, *J. Am. Chem. Soc.*, 2023, **145**, 13537–13541.
11 T. Jadhav, Y. Fang, C.-H. Liu, A. Dadvand, E. Hamzehpoor, W. Patterson, A. Jonderian, R. S. Stein and D. F. Perepichka, *J. Am. Chem. Soc.*, 2020, **142**, 8862–8870.
12 Y. Meng, Y. Luo, J. L. Shi, H. Ding, X. Lang, W. Chen, A. Zheng, J. Sun and C. Wang, *Angew. Chem.*, 2020, **132**, 3653–3658.
13 H. L. Nguyen, *Chem. Sci.*, 2021, **12**, 8632–8647.
14 K. Zheng, Z. Gou, C. Zhang, Y. Zhang, Y. Dou, S. Liu, Y. Zhang and Y. Zhang, *Chem. Sci.*, 2024, **15**, 19160–19167.
15 C. Wang, Z. Zhang, Y. Zhu, C. Yang, J. Wu and W. Hu, *Adv. Mater.*, 2022, **34**, 2102290.

16 R.-R. Liang, S.-Y. Jiang, R.-H. A and X. Zhao, *Chem. Soc. Rev.*, 2020, **49**, 3920–3951.
17 S. S. A. Shah, M. S. Javed, T. Najam, M. A. Nazir, A. ur Rehman, A. Rauf, M. Sohail, F. Verpoort and S.-J. Bao, *Mater. Today*, 2023, **67**, 229–255.
18 S.-Y. Ding and W. Wang, *Chem. Soc. Rev.*, 2013, **42**, 548–568.
19 A. P. Côté, A. I. Benin, N. W. Ockwig, M. O'Keeffe, A. J. Matzger and O. M. Yaghi, *Science*, 2005, **310**, 1166–1170.
20 H. M. El-Kaderi, J. R. Hunt, J. L. Mendoza-Cortés, A. P. Côté, R. E. Taylor, M. O'Keeffe and O. M. Yaghi, *Science*, 2007, **316**, 268–272.
21 N. Brown, Z. Alsudairy, R. Behera, F. Akram, K. Chen, K. Smith-Petty, B. Motley, S. Williams, W. Huang, C. Ingram and X. Li, *Green Chem.*, 2023, **25**, 6287–6296.
22 B. P. Biswal, S. Chandra, S. Kandambeth, B. Lukose, T. Heine and R. Banerjee, *J. Am. Chem. Soc.*, 2013, **135**, 5328–5331.
23 S. Kandambeth, K. Dey and R. Banerjee, *J. Am. Chem. Soc.*, 2018, **141**, 1807–1822.
24 T. Liu, Y. Zhao, M. Song, X. Pang, X. Shi, J. Jia, L. Chi and G. Lu, *J. Am. Chem. Soc.*, 2023, **145**, 2544–2552.
25 H. Li, J. Fan, M. Ran, R. A. Borse, S. X. Lin and D. Yuan, *Angew. Chem., Int. Ed.*, 2025, **64**, e202500937.
26 M. Liu, H. Y. Kong, S. Bi, X. Ding, G. Z. Chen, J. He, Q. Xu, B. H. Han and G. Zeng, *Adv. Funct. Mater.*, 2023, **33**, 2302637.
27 B. Hou, S. Yang, K. Yang, X. Han, X. Tang, Y. Liu, J. Jiang and Y. Cui, *Angew. Chem., Int. Ed.*, 2021, **60**, 6086–6093.
28 W. Zhao, C. Yu, J. Zhao, F. Chen, X. Guan, H. Li, B. Tang, G. Yu, V. Valtchev, Y. Yan, S. Qiu and Q. Fang, *Small*, 2021, **17**, 2102630.
29 F. J. Uribe-Romo, J. R. Hunt, H. Furukawa, C. Klöck, M. O'Keeffe and O. M. Yaghi, *J. Am. Chem. Soc.*, 2009, **131**, 4570–4571.
30 T. Ma, J. Li, J. Niu, L. Zhang, A. S. Etman, C. Lin, D. Shi, P. Chen, L.-H. Li, X. Du, J. Sun and W. Wang, *J. Am. Chem. Soc.*, 2018, **140**, 6763–6766.
31 K. Geng, T. He, R. Liu, S. Dalapati, K. T. Tan, Z. Li, S. Tao, Y. Gong, Q. Jiang and D. Jiang, *Chem. Rev.*, 2020, **120**, 8814–8933.
32 Y. Li, W. Chen, G. Xing, D. Jiang and L. Chen, *Chem. Soc. Rev.*, 2020, **49**, 2852–2868.
33 E. Hamzehpoor, F. Effaty, T. H. Borchers, R. S. Stein, A. Wahrhaftig-Lewis, X. Ottenwaelder, T. Friščić and D. F. Perepichka, *Angew. Chem., Int. Ed.*, 2024, **63**, e202404539.
34 S. T. Emmerling, L. S. Germann, P. A. Julien, I. Moudrakovski, M. Etter, T. Friščić, R. E. Dinnebier and B. V. Lotsch, *Chem*, 2021, **7**, 1639–1652.
35 L. Bourda, C. Krishnaraj, P. Van Der Voort and K. Van Hecke, *Mater. Adv.*, 2021, **2**, 2811–2845.
36 F. Haase and B. V. Lotsch, *Chem. Soc. Rev.*, 2020, **49**, 8469–8500.
37 Y. Chen, Z.-L. Shi, L. Wei, B. Zhou, J. Tan, H.-L. Zhou and Y.-B. Zhang, *J. Am. Chem. Soc.*, 2019, **141**, 3298–3303.
38 X.-L. Wang, L.-T. Zhang, S. He, X.-X. Chen, X.-C. Huang and H.-L. Zhou, *Chem. Mater.*, 2023, **35**, 10070–10077.
39 Z. Zhou, L. Zhang, Y. Yang, I. J. Vitorica-Yrezabal, H. Wang, F. Tan, L. Gong, Y. Li, P. Chen, X. Dong, Z. Liang, J. Yang, C. Wang, Y. Hong, Y. Qiu, A. Gölzhäuser, X. Chen, H. Qi, S. Yang, W. Liu, J. Sun and Z. Zheng, *Nat. Chem.*, 2023, **15**, 841–847.
40 K. Wang, B. Hou, J. Dong, H. Niu, Y. Liu and Y. Cui, *J. Am. Chem. Soc.*, 2024, **146**, 21466–21475.
41 M. Gupta and J. J. Vittal, *Coord. Chem. Rev.*, 2021, **435**, 213789.
42 D. R. Du Bois and A. J. Matzger, *Cryst. Growth Des.*, 2022, **22**, 6379–6383.
43 L. Feng, K.-Y. Wang, T.-H. Yan and H.-C. Zhou, *Chem. Sci.*, 2020, **11**, 1643–1648.
44 Y. Hu, W.-K. Han, Y. Liu, R.-M. Zhu, X. Yan, H. Pang and Z.-G. Gu, *ACS Mater. Lett.*, 2023, **5**, 2534–2541.
45 H. Chen, D. Feng, F. Wei, F. Guo and A. K. Cheetham, *Angew. Chem., Int. Ed.*, 2024, **64**, e202415454.
46 T. Yang, T. Willhammar, H. Xu, X. Zou and Z. Huang, *Nat. Protoc.*, 2022, **17**, 2389–2413.
47 T. Yang, H. Xu and X. Zou, *J. Appl. Crystallogr.*, 2022, **55**, 1583–1591.
48 Z. P. Lv, D. Srivastava, K. Conley, T. P. Ruoko, H. Xu, M. Lightowler, X. Hong, X. Cui, Z. Huang, T. Yang, H. Y. Wang, A. J. Karttunen and L. Bergström, *Small Methods*, 2024, **8**, 2301229.
49 T. Sun, L. Wei, Y. Chen, Y. Ma and Y.-B. Zhang, *J. Am. Chem. Soc.*, 2019, **141**, 10962–10966.
50 F. Wang, Y. Chen, T. Gong and J. Gong, *ACS Macro Lett.*, 2023, **12**, 1576–1582.
51 X. Liu, Z. Wang, Y. Zhang, N. Yang, B. Gui, J. Sun and C. Wang, *J. Am. Chem. Soc.*, 2024, **146**, 11411–11417.
52 J. Liu, Y. Chen, X. Su and J. Gong, *Mater. Chem. Front.*, 2022, **6**, 3504–3511.
53 Y.-B. Zhang, J. Su, H. Furukawa, Y. Yun, F. Gándara, A. Duong, X. Zou and O. M. Yaghi, *J. Am. Chem. Soc.*, 2013, **135**, 16336–16339.
54 X. Shi, Z. Zhang, M. Wei, X. Wang, J. Wang, Y. Zhang and Y. Wang, *Macromolecules*, 2022, **55**, 3259–3266.